

Chapter 2

Evolution of the Solar/Stellar Radiation and Plasma Environment

The evolution of planetary atmospheres can only be understood if one considers that the radiation and particle environment of the Sun or a planet's host star changed during their life time. The magnetic activity of solar-type stars declines steadily during their evolution on the Zero-Age-Main-Sequence (ZAMS). According to the solar standard model, the Sun's photospheric luminosity was $\sim 30\%$ lower ~ 4.5 Gyr ago when the Sun arrived on the ZAMS compared to present levels. The observed faster rotation of young stars is responsible for an enhanced magnetic activity and related heating processes in the chromosphere, X-ray emissions are $\geq 1,000$, and EUV, and UV ~ 100 and ~ 10 times higher compared to today's solar values. Moreover, the production rate of high-energy particles is orders of magnitude higher at young stars, and from observable stellar mass loss-activity relations one can also expect a much stronger solar/stellar wind during the active stellar phase. The interaction with these high-energy radiation and the solar/stellar wind plasma interaction with upper planetary atmospheres modifies the thermospheric density and temperature structure and effects finally the whole planetary evolution due to thermal and non-thermal atmospheric escape processes [1].

2.1 Solar/Stellar-Atmospheric Temperature Relations

The effective temperature T_{eff} of a planetary surface in the absence of an atmosphere can be derived from the energy balance between the optical/near infrared emission which irradiates the planet and the mid-infrared (IR) thermal radiation that is lost to space

$$T_{\text{eff}} = \left[\frac{S(1 - A)}{4\sigma_B \varepsilon} \right]^{\frac{1}{4}}, \quad (2.1)$$

with S the flux density of incoming solar/stellar electromagnetic radiation per unit area that would be incident on a plane perpendicular to the rays, at the planet's

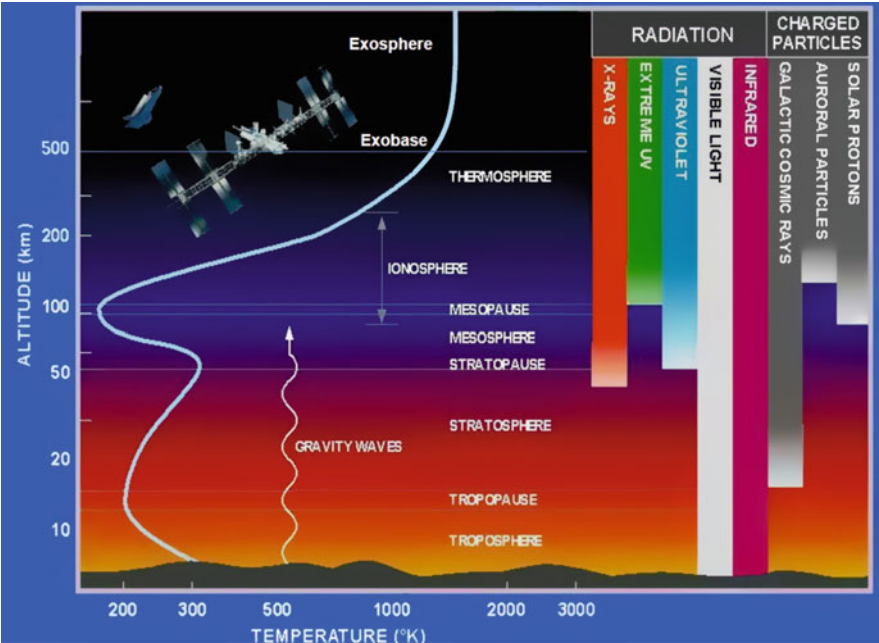


Fig. 2.1 Illustration of the Earth’s temperature profiles, atmospheric regions, and incoming solar radiation. Longer wavelengths reach the surface and control a planet’s climate, while shorter wavelengths are absorbed in the upper atmosphere and control the thermosphere and exobase temperature

distance in AU (for the Earth: solar constant), σ_B the Stefan-Boltzmann constant, the planet’s albedo A and the surface mid-IR emissivity ε . If a planet has an atmosphere, T_{eff} can be higher due to the presence of greenhouse gases. Greenhouse gases such as H_2O , CH_4 , CO_2 are nearly transparent to the incident optical and near-infrared (IR) radiation but strongly absorb re-emitted thermal radiation in the mid-IR. The Earth’s present day atmosphere leads to a greenhouse effect which results in a daily average surface temperature of about $\sim 288\text{ K}$ [2].

The optical and infrared emissions of young stars largely control the lower regions of a planetary atmosphere (e.g., troposphere, mesosphere) and their related climate. The more energetic shorter wavelength emissions of X-ray, soft X-ray (SXR), EUV photons as well as the interaction with high-energy particles, the stellar wind, or coronal mass ejections (CMEs) lead to heating and expansion of the upper atmospheres [3, 4].

As illustrated in Fig. 2.1 the heat production by the incoming solar/stellar EUV radiation in a planet’s upper atmosphere is balanced by the divergence of the conductive heat flux of the EUV radiation. In the so-called thermosphere the short wavelength radiation of is absorbed and transferred partly into heating which leads to a positive temperature gradient. The heat transport in the lower part of the thermosphere

Table 2.1 Average surface, effective and exobase temperatures of Venus, Earth and Mars

Planets	T_s (K)	T_{eff} (K)	T_{exo} (K)
Venus	~735	~232	~270
Earth	~232	~254	~900
Mars	~215	~210	~220

is dominated by convection, while in the upper part heat transport by conduction takes over, which leads to an isothermal region. The altitude in this region where the mean free part of the atmospheric species becomes equal to their scale height is called the exobase level, which separates the upper atmosphere in a collision-dominated and a collision-less region. The exobase temperature T_{exo} can be analytically be written as [5]

$$T_{\text{exo}}^s = \frac{s \eta \alpha k}{K_0 m_i g} \int_{\lambda_1}^{\lambda_2} d\lambda I_{\text{EUV}}(\lambda) \left\{ E[\tau(\lambda)] + \ln[\tau(\lambda)] + \gamma - \frac{m_i}{m_j} \left[1 - e^{-\tau(\lambda)} \right] \right\} + T_0^s, \quad (2.2)$$

where λ is the wavelength, I_{EUV} is the EUV intensity at the orbit location, τ is the optical thickness, E is the exponential integral, γ is Euler's constant, η is the EUV heating efficiency of the gas, k is the Boltzmann constant, m_i and m_j are the masses of the main atmospheric constituents, $K(T) = K_0 T^s$ is the thermal conductivity coefficient, s depends on the thermospheric composition, g is the gravitational acceleration, and T_0 is the temperature at the base of the thermosphere which is $\approx T_{\text{eff}}$. In the case of a hydrogen-dominated thermosphere $i \approx j$ [5]. The factor α is connected to the rotation of the planet and is ~ 0.25 for rapidly rotating planets and ~ 0.5 for slowly rotating or tidally locked planets [5, 6]. With some approximations, T_{exo} can be expressed in a less complex formula [6–9]:

$$T_{\text{exo}}^s \approx \frac{\eta \alpha I_{\text{EUV}} k \sigma_c}{K_0 m_i g \sigma_a} + T_0^s, \quad (2.3)$$

where σ_c and σ_a are the collision and absorption cross-sections. Table 2.1 compares the average surface temperature T_s , the average exobase temperature T_{exo} with the average T_{eff} of Venus, the Earth and Mars. One can see from Table 2.1 that due to the extreme greenhouse effect in Venus' atmosphere the planet's surface temperature is much larger compared to that of Earth and Mars, while the effective temperatures of all three planets are not so different. One can also see that the N_2 -dominated atmosphere of the present Earth has a much higher exobase temperature compared to the CO_2 -rich upper atmospheres of Venus and Mars. Contrary to nitrogen, CO_2 is a greenhouse gas and also an efficient IR-cooler in the upper atmosphere.

Table 2.2 The evolution of the solar luminosity L , effective temperature T_{eff} , and radius r from the ZAMS until the beginning of the Sun's red giant phase normalized to the present day values [11]

Solar age (Gyr)	L/L_{Sun}	$T_{\text{eff}}/T_{\text{Sun}}$	r/r_{Sun}
0	~ 0.7	~ 0.9	~ 0.85
~ 2	~ 0.8	~ 0.95	~ 0.9
~ 4	~ 0.9	~ 0.97	~ 0.93
~ 4.5	1	1	1
~ 6	~ 1.05	~ 1	~ 1.05
~ 8	~ 1.3	~ 1	~ 1.15
~ 10	~ 1.95	~ 0.98	~ 1.5

2.2 Radiation Environment of the Young Sun/Stars

The nuclear evolution of the Sun is well known from stellar evolutionary theory and backed by helioseismological observations of the internal solar structure [10]. The results of these evolutionary solar models, indicate that the young Sun was $\sim 10\%$ cooler and $\sim 15\%$ smaller compared to the modern Sun ~ 4.6 Gyr ago. According to the solar standard model, due to accelerating nuclear reactions in the Sun's core, the Sun is a slowly evolving variable G-type star that has undergone an $\sim 30\%$ increase in luminosity over the past ~ 4.5 Gyr. In ~ 0.1 Gyr from today, the Sun will be $\sim 10\%$ brighter, so that the Earth will be heated enough that the oceans start to evaporate. In ~ 6 Gyr from now the Sun expands beyond the Earth's orbit to become a red giant [11, 12]. The evolution of the Sun's luminosity L , effective temperature, T_{eff} , and radius r after it arrived at the ZAMS to the beginning of the red giant phase are shown in Table 2.2. According to these values the onset of ocean evaporation begins at a solar age of ~ 5.8 Gyr and the runaway greenhouse effect occurs at ~ 8.5 Gyr. From these parameters the young Sun may have had an initial luminosity of $\sim 70\%$ of the present Sun resulting in a significantly lower solar constant.

Table 2.3 lists the short wavelength radiation fluxes of the Sun as reconstructed from observed solar proxies as a function of age between ~ 0.1 and 4.6 Gyr. The fluxes are divided into six wavelength intervals and normalized to the values of the modern Sun [4, 13, 14]. One can see from Table 2.3 that the sample of well-studied solar proxies contain six nearby G0V-G5V stars. The solar analogs EK Dra, π^1 UMa, HN Peg, χ^1 Ori, BE Cet, and κ^1 Cet have known rotation periods, temperatures, luminosities, and metallicities which fall into the early age domain of the Sun to $t \leq 0.65$ Gyr [4, 13].

The observational data of these solar proxies with ages < 0.1 Gyr reveal that the EUV flux is saturated at ~ 100 times of the average present time solar value during the first ~ 100 Myr [15]. After that very active period the EUV flux decreases with time t in units of Gyr according to an empirical scaling law which can be written as [13, 14]

$$S_{\text{EUV}} = \left(\frac{t_{\text{[Gyr]}}}{t_{\text{Sun[Gyr]}}} \right)^{-1.23}. \quad (2.4)$$

Table 2.3 Solar/stellar radiation flux enhancement factors obtained from observations of solar proxies as function of wavelength normalized to the present solar value from today to ~ 4.5 Gyr ago [4, 13, 14]

Solar age (Gyr)	t b.p. (Gyr)	X-ray (0.1–2 nm)	SXR (2–10 nm)	EUV (10–92 nm)	FUV (92–118 nm)	Lyman- α (120–130 nm)
4.6	0	1	1	1	1	1
3.2	1.4	2	1.6	1.5	1.4	1.3
2.6	2	3	2	1.9	1.6	1.5
1.9	2.7	6	3	2.7	2.1	1.9
1.1	3.5	16	6	5.1	3.4	2.8
0.7	3.9	37	11	8.6	5	3.9
0.65	3.95	43	12	9.4	5.3	4.1
0.6	4.0	50	13	10	5.7	4.3
0.55	4.05	59	15	11	6.1	4.6
0.5	4.1	71	17	13	6.6	4.9
0.45	4.15	87	19	14	7.2	5.3
0.4	4.2	109	22	17	8	5.8
0.35	4.25	141	26	19	9	6.4
0.3	4.3	189	32	23	10	7.1
0.25	4.35	268	40	28	12	8.1
0.2	4.4	412	54	37	14	9.6
0.15	4.45	715	77	51	18	11.8
0.1	4.5	1558	129	82	26	15.8

with the EUV flux enhancement factor S_{EUV} and t_{Sun} the age of the Sun in units of Gyr. It should be noted that by expanding the activity-age relation from solar mass to lower mass stars one finds that lower mass stars spend more time in the saturated level before their activity decays [16] and stars of the same spectral type show a wider distribution of the X-ray luminosity [17]. By using ROSAT satellite measurements of G-type stars which cover the transition region in wavelength λ between SXR and EUV ($\lambda \sim 10$ nm) one can construct scaling laws based from the ROSAT data which reproduce the EUV and SXR luminosity evolution as a valid EUV proxy [17–20]. These scalings are justified because the SXR data correlate well with measurements of the EUVE satellite in the wavelength range of ~ 10 – 36 nm shown for the solar proxies in Table 2.2. From this relation one can also construct generalized EUV scaling laws for F, G, K, and M-type stars for L_{SXR} in units of erg s^{-1} . The temporal evolution of the stellar SXR flux at a planetary orbit and r_{pl} are taken into account, while the stellar mass and orbital distance d are assumed to be constant. For the range of general F stars with $L_0 = 10^{29.83}$ one obtains [19],

$$\begin{aligned}
 L_{\text{SXR}} &= 0.284 L_0 t^{-0.547} t \leq 0.6 \text{ Gyr}, \\
 L_{\text{SXR}} &= 0.155 L_0 t^{-1.72} t > 0.6 \text{ Gyr},
 \end{aligned}
 \tag{2.5}$$

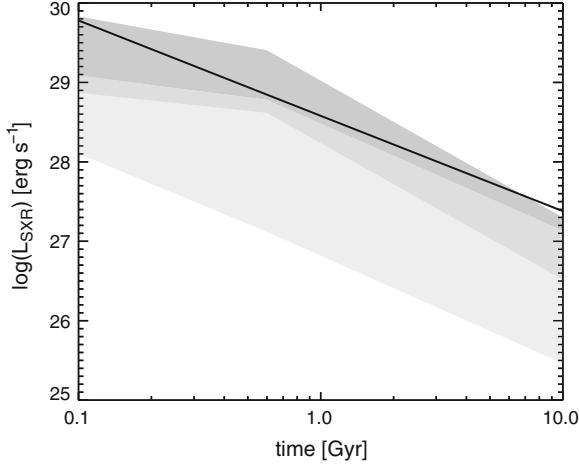


Fig. 2.2 Average SXR luminosity L_{SXR} in units of erg s^{-1} as a function of stellar age for G- and F-type stars (*dark gray area*), K and M stars (*bright gray area*) [19] at 1 AU. The *solid line* represents the result from the power law analyzed from EUVE satellite data of solar proxies with different ages [13]. The *dark gray* together with the *gray area* correspond to the standard deviation 1σ of the G-star distribution, and *light gray* together with the *gray area* to the standard deviation 1σ of M-type stars. Both distributions are overlapped by the *gray area*

for G-stars with $L_0 = 10^{29.35}$,

$$\begin{aligned} L_{\text{SXR}} &= 0.375L_0t^{-0.425}t \leq 0.6 \text{ Gyr}, \\ L_{\text{SXR}} &= 0.19L_0t^{-1.69}t > 0.6 \text{ Gyr}, \end{aligned} \quad (2.6)$$

for K-type stars, $L_0 = 10^{28.87}$,

$$\begin{aligned} L_{\text{SXR}} &= 0.474L_0t^{-0.324}t \leq 0.6 \text{ Gyr}, \\ L_{\text{SXR}} &= 0.234L_0t^{-1.72}t > 0.6 \text{ Gyr}, \end{aligned} \quad (2.7)$$

and for M dwarfs, $L_0 = 10^{28.75}$,

$$\begin{aligned} L_{\text{SXR}} &= 0.17L_0t^{-0.77}t \leq 0.6 \text{ Gyr}, \\ &0.13L_0t^{-1.34}t > 0.6 \text{ Gyr}. \end{aligned} \quad (2.8)$$

The stellar age t is in units of Gyr and $F_{\text{EUV}} \approx L_{\text{SXR}}/4\pi d^2$ [19]. Figure 2.2 shows the SXR luminosity evolution obtained from the above-mentioned scaling laws for G, F, K, and M-type dwarf stars as a function of stellar age at an orbital distance of 1 AU. One can see that stars with lower masses remain somewhat longer at active emissions compared to solar-like G-type stars. After their high activity phase the emissions decrease by a similar power law relationship as that of the solar proxies shown in

Table 2.3. In addition to the short wavelength radiation, which can heat and expand upper atmospheres the solar/stellar wind, as well as coronal mass ejections (CMEs) will also result in permanent forcing of the thermosphere-exosphere-magnetosphere environment during the early phase of a planet's lifetime.

2.3 Evolution of the Solar/Stellar Wind with Time

Because the outward flowing plasma carries away angular momentum from the star one of the best indirect confirmation that the plasma outflow from young stars is very efficient is the observed spin-down to slower rotation of young stars after their arrival at the ZAMS. Stellar wind and CME-related plasma are ejected from the star but the observation of such features at solar proxies is very difficult [4, 21–23]. Detection methods of stellar winds include the measurement of thermal radio emission from the plasma flow [24, 25], and signatures of charge exchange in X-ray spectra [26].

The most successful approach so far is an indirect method which observes the Lyman- α absorption in astrospheres caused by neutral hydrogen atoms which are produced from the interaction between stellar wind plasma and the interstellar medium (ISM) [22, 23]. A termination shock forms when stellar winds collide with the ISM at further distance from the star and the wind is shocked to subsonic velocities [21–23]. Much of the gas is piled up between the heliopause and the bow shock. As a result a hydrogen wall is produced and its signature in the Lyman- α line of neutral H atoms can be observed. The measurable absorption depths in the Lyman- α line are then compared with results from hydrodynamic model calculations [23].

A systematic study of all derived stellar mass-loss rates of main sequence stars which were observed with this method indicates that the mass loss as a function of time dM_L/dt per unit stellar surface correlates well with the stellar activity and the stellar X-ray surface flux, $F_{X\text{-ray}}$ [23]

$$\frac{dM_L}{dt} \propto F_{X\text{-ray}}^{1.34 \pm 0.18}. \quad (2.9)$$

When one extrapolates the above power law up to the observed X-ray saturation limit of the Sun-like stars of $\sim 2 \times 10^7 \text{ erg cm}^{-2} \text{ s}^{-1}$, one would suggest that the average mass loss of plasma from the youngest stars such as these shown in Table 2.3 is more than $\sim 1,000$ times larger compared to the mass loss of the present Sun. However, until now there are no accurate mass loss observations of young solar-like single stars available. To avoid wrong estimations the power law relation given in Eq. 2.9 should not be applied for the most active stars for which $F_X \geq 8 \times 10^5 \text{ erg cm}^{-2} \text{ s}^{-1}$ [23].

A possible reason that the mass loss-X-ray activity power law relation fails for very young solar-type stars could be related to the fast rotation period of young stars of a few days during the first 500 Myr after the arrival at the ZAMS because the activity and magnetic field configuration was most likely quite different from the

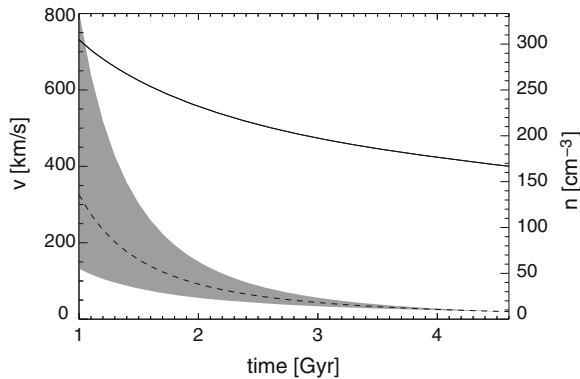


Fig. 2.3 Dashed-line average stellar wind density and velocity (solid line) estimated from stellar mass loss observations at 1 AU between 1 Gyr and present time (4.6 Gyr)

current appearance [27, 28]. In such a case the Sun spots at latitudes which are $\geq 60^\circ$ degree could change the structure of coronal magnetic fields as well as the formation of prominences, which might lead to a predominant occurrence of flares and CMEs at high latitudes which may propagate significantly above the ecliptical plane. For studying the effect on planetary environments against solar/stellar wind-induced non-thermal escape, the solar/stellar wind density and velocity in the vicinity of a planet are key parameters. The age dependence of the solar/stellar wind velocity for the Sun-like stars can be estimated from the stellar mass loss observations discussed above, in combination with an empirical models [4, 29–31]. The shaded area in Fig. 2.3 represents uncertainties of the solar wind density in time which shows the expected enhancement in solar wind density and velocity, according to mass loss observations of the Sun-like stars [23] and the power laws [31] as function of age from present time back to ~ 3.5 Gyr ago. From the observational evidence of the stellar radiation and plasma environment one can expect that these photon and particle fluxes certainly have an impact on the origin and early evolution of planetary atmospheres.

References

1. Lundin, R., Lammer, H., Ribas, I.: Planetary magnetic fields and solar forcing: implications for atmospheric evolution. *Space Sci. Rev.* **129**, 245–278 (2007)
2. Sagan, C., Mullen, G.: Earth and Mars: evolution of atmospheres and surface temperatures. *Science* **177**, 52–56 (1972)
3. Krauss, S., Fichtinger, B., Lammer, H., Hausleitner, W., Kulikov, Yu. N., Ribas, I., Schematovich, V.I., Bisikalo, D., Lichtenegger, H.I.M., Zaqarashvili, T.V., Khodachenko, M.L., Hanslmeier, A.: Solar flares as proxy for the young Sun: satellite observed thermosphere response to an X17.2 flare of Earth's upper atmosphere. *Ann. Geophys.* **30**, 1129–1141 (2012)
4. Lammer, H., Güdel, M.: Kulikov, YuN, Ribas, I., Zaqarashvili, T.V., Khodachenko, M.L., Kislyakova, K.G., Gröller, H., Odert, P., Leitzinger, M., Fichtinger, B., Krauss, S., Hausleitner,

- W., Holmström, M., Sanz-Forcada, J., Lichtenegger, H.I.M., Hanslmeier, A., Shematovich, V.I., Bisikalo, D., Rauer, H., Fridlund, M.: Variability of solar/stellar activity and magnetic field and its influence on planetary atmosphere evolution. *Earth Planets Space* **63**, 179–199 (2012)
5. Gross, S.H.: On the exospheric temperature of hydrogen-dominated planetary atmospheres. *J. Atmos. Sci.* **29**, 214–218 (1972)
6. Bauer, S.J.: *Physics of Planetary Ionospheres*. Springer, Berlin (1973)
7. Bauer, S.J.: Solar cycle variation of planetary exospheric temperatures. *Nature* **232**, 101–102 (1971)
8. Lammer, H., Selsis, F., Ribas, I., Guinan, E.F., Bauer, S.J., Weiss, W.W.: Atmospheric loss of exoplanets resulting from stellar X-Ray and extreme-ultraviolet heating. *ApJ* **598**, L121–L124 (2003)
9. Bauer, S.J., Lammer, H.: *Planetary Aeronomy: Atmosphere Environments in Planetary Systems*. Springer, Berlin (2004)
10. Guzik, J.A., Watson, L.S., Cox, A.N.: Implications of revised solar abundances for helioseismology. *Memorie della Societa Astronomica Italiana* **77**, 389–392 (2006)
11. Bressan, A., Fagotto, F., Bertelli, G., Chiosi, C.: Evolutionary sequences of stellar models with new radiative opacities. II - $Z=0.02$. *Astron. Astrophys. Suppl. Ser.* **100**, 647–664 (1993)
12. Kasting, J.F.: Runaway and moist greenhouse atmospheres and the evolution of Earth and Venus. *Icarus* **74**, 472–494 (1988)
13. Ribas, I., Guinan, E.F., Güdel, M., Audard, M.: Evolution of the solar activity over time and effects on planetary atmospheres. I. High-energy irradiances (1–1700 Å). *ApJ* **622**, 680–694 (2005)
14. Güdel, M.: The sun in time: activity and environment. *Living Rev. Sol. Phys.* **4**(3), 1–137 (2007)
15. Güdel, M., Guinan, E.F., Skinner, S.L.: The X-ray sun in time: a study of the long-term evolution of coronae of solar-type stars. *ApJ* **483**, 947–960 (1997)
16. Scalo, J., Kaltenecker, L., Segura, A.G., Fridlund, M., Ribas, I., Kulikov, Yu.N., Grenfell, J.L., Rauer, H., Odert, P., Leitzinger, M., Selsis, F., Khodachenko, M.L., Eiroa, C., Kasting, J., Lammer, H.: M stars as targets for terrestrial exoplanet searches and biosignature detection. *Astrobiology* **7**, 85–166 (2007)
17. Penz, T., Micela, G., Lammer, H.: Influence of the evolving stellar X-ray luminosity distribution on exoplanetary mass loss. *Astron. Astrophys.* **477**, 309–314 (2008)
18. Penz, T., Micela, G.: X-ray induced mass loss effects on exoplanets orbiting dM stars. *Astron. Astrophys.* **479**, 579–584 (2008)
19. Lammer, H., Odert, P., Leitzinger, M., Khodachenko, M.L., Panchenko, M., Kulikov, Yu.N., Zhang, T.L., Lichtenegger, H.I.M., Erkaev, N.V., Wuchterl, G., Micela, G., Penz, A., Biernat, H.K., Weingrill, J., Steller, M., Ottacher, H., Hasiba, J., Hanslmeier, A.: Determining the mass loss limit for close-in exoplanets: what can we learn from transit observations? *A&A* **506**, 399–410 (2009)
20. Lammer, H., Bredehöft, J.H., Coustenis, A., Khodachenko, M.L., Kaltenecker, L., Grasset, O., Prieur, D., Raulin, F., Ehrenfreund, P., Yamauchi, M., Wahlund, J.-E., Grießmeier, J.-M., Stangl, G., Cockell, C.S., Kulikov, Yu.N., Grenfell, L., Rauer, H.: What makes a planet habitable? *Astron. Astrophys. Rev.* **17**, 181–249 (2009)
21. Wood, B.E., Müller, H.-R., Zank, G., Linsky, J.L.: Measured mass loss rates of solar-like stars as a function of age and activity. *ApJ* **574**, 412–425 (2002)
22. Wood, B.E.: Astrospheres and solar-like stellar winds. *Living Rev. Sol. Phys.* **1**(2), 1–44 (2004)
23. Wood, B.E., Müller, H.-R., Zank, G.P., Linsky, J.L., Redfield, S.: New mass loss measurements from astrospheric Ly- α absorption. *ApJ* **628**, L143–L146 (2005)
24. Lim, J., White, S.M.: Limits to mass outflows from late-type dwarf stars. *ApJL* **462**, L91–L94 (1996)
25. Gaidos, E.J., Güdel, M., Blake, G.A.: The faint young Sun paradox: an observational test of an alternative solar model. *Geophys. Res. Lett.* **27**, 501–503 (2000)

26. Wargelin, B.J., Drake, J.J.: Observability of stellar winds from late-type dwarfs via charge exchange X-ray emission. *ApJL* **546**, L57–L60 (2001)
27. Zaqarashvili, T.V., Oliver, R., Ballester, J.L., Carbonell, M., Khodachenko, M.L., Lammer, H., Leitzinger, M., Odert, P.: Rossby waves and polar spots in rapidly rotating stars: implications for stellar wind evolution. *A and A* **532**, A139 (2011)
28. Zaqarashvili, T.V., Carbonell, M., Oliver, R., Ballester, J.L.: Quasi-biennial oscillations in the solar tachocline caused by magnetic Rossby wave instabilities. *ApJL* **724**, L95–L98 (2011)
29. Grießmeier, J.M., Motschmann, U., Stadelmann, A., Penz, T., Lammer, H., Selsis, F., Ribas, I., Guinan, E.F., Biernat, H.K., Weiss, W.W.: The effect of tidal locking on the magnetospheric and atmospheric evolution of “Hot Jupiter”. *Astron. Astrophys.* **425**, 618–630 (2007)
30. Grießmeier, J.-M., Preusse, S., Khodachenko, M., Motschmann, U.: Exoplanetary radio emission under different stellar wind conditions. *Planet. Space Sci.* **55**, 618–630 (2007)
31. Newkirk Jr., G.: Solar variability on time scales of 10^5 years to $10^{9.6}$ years. *Geochi. Cosmochi. Acta Suppl.* **13**, 293–301 (1980)

Origin and Evolution of Planetary Atmospheres
Implications for Habitability

Lammer, H.

2013, XVI, 98 p. 37 illus., 23 illus. in color., Softcover

ISBN: 978-3-642-32086-6